ISSN 1392-1320 MATERIALS SCIENCE (MEDŽIAGOTYRA). Vol. XX, No. X. 2025

On the Influence of Microstructure and Properties of Direct Laser Deposited 50Cr6Ni2Y Coatings with Different TiC Contents

Xueting CHEN *, Zichun YU, Zhanqi LIU, Guili YIN

School of Materials Science and Engineering, Liaoning University of Technology, Jinzhou 121001, China

http://doi.org/10.5755/j02.ms.38044

Received 29 July 2014; accepted 27 September 2024

Three 50Cr6Ni2Y + x wt.% TiC (x = 1.5, 3.0, 4.5) alloy steel coatings were prepared using direct laser deposition (DLD) technology. The microstructure, microhardness, and wear resistance of DLD samples were studied. The results indicate that DLD coatings were composed of α-Fe (Fe-Cr-Ti), γ-Fe (Fe-Ni), and TiC. When the added TiC content was 3.0 wt.%, the DLD coating without cracks was fabricated, and TiC particles were well embedded in the sample. In addition, the coating demonstrated the best performance, with a microhardness of 758 ± 23.3 $HV_{0.2}$, an average friction coefficient of 0.58, and a wear rate of 0.37 %. The addition of an appropriate amount of TiC as a reinforcing phase, on the one hand, had played a role in the second phase strengthening. On the other hand, the diffusion interfaces formed between TiC particles and the matrix allowed some Ti elements to melt into the matrix and formed a solid solution, playing a role in solid solution strengthening. The results could provide a reference for the preparation and repair of laser additive manufacturing high-performance wear-resistant parts.

Keywords: direct laser deposition, medium carbon steel, TiC, microstructure, wear resistance.

1. INTRODUCTION

Direct laser deposition (DLD) is a process that utilizes high-energy-density laser beams to heat and rapidly melt metal surfaces, allowing for the layer-by-layer creation of parts [1, 2]. DLD can be used to reinforce coatings with excellent wear and corrosion resistance on the surface of parts [3]. DLD technology has shown broad application prospects in the preparation and repair of surface coatings on wear-resistant parts [4, 5]. Especially for wear-resistant parts widely used in industry, such as short stress line rolling mills, high-speed rail brake discs, nuclear emergency diesel generators, etc. The surface working layer of these parts has the characteristics of high hardness (700 – 900 HV) and good wear resistance. Therefore, the alloy steel composite powder that can meet the high hardness requirements of the surface working layer deserves further research. With the increasing demand for high-strength and wear-resistant materials for wear-resistant parts, we designed a 50Cr6Ni2Y alloy steel powder in our previous research [6]. The DLD 50Cr6Ni2Y alloy steel can be used as an intermediate layer for wear-resistant parts with an average hardness of 534 HV, a tensile strength of 1139 MPa, and an elongation of 2 %. Therefore, it is necessary to change the composition of 50Cr6Ni2Y powder to improve the strength and obtain a coating with high hardness on the surface of wear-resistant parts.

Reinforcement phases such as oxides, carbides, nitrides, borides, etc. are usually added to the coating to improve the hardness and wear resistance of coatings [7, 8]. TiC is widely added to improve the performance of laser additive manufacturing coatings due to its excellent physical properties, high wear resistance, oxidation resistance, and high corrosion resistance [9 – 11]. For example, the research results of Xu [12] et al. indicate that adding an appropriate amount of TiC can significantly enhance the Inconel 625 composite coating. The microhardness and tensile strength of the reinforced coating with TiC were significantly improved compared with the Inconel 625. Zhang [13] et al. found that TiC particles play a role in fine grain strengthening and second phase strengthening in the TiC modified iron-based composite coating. The average microhardness of the coating was 703 ± 17 HV. The specific wear rate was 4.0×10^{-6} $mm^3/N \cdot m$, which was smaller than that of the substrate (2.2×10^{-5} $mm^3/N \cdot m$). Liu [14] et al. also reported that TiC particles can improve the properties of 316L steel. It was found that the TiC particles were uniformly distributed in the microstructure, which was helpful to improve the mechanical properties, hardness and wear resistance of the coating.

The results of above researchs indicate that TiC particles can bind well with coatings and significantly improve the hardness and wear resistance. Therefore, three 50Cr6Ni2Y alloy coatings with different TiC contents were prepared by DLD in this paper. The effect of TiC on the microstructure, microhardness, wear resistance, and strengthening mechanism needs to be studied, and the strengthening mechanism needs to be further clarified. It is expected to obtain a high-hardness and wear-resistance coating with good laser formability. The results could provide a reference for the preparation and repair of laser additive manufacturing high-performance wear-resistant parts.

2. EXPERIMENTAL MATERIALS AND METHODS

2.1. DLD process

Q235 was used as the base material which was 100 mm × 100 mm × 10 mm in size. The experimental

* Corresponding author. Tel.: +86-0416-4199779; fax: +86-0416-4198642. E-mail: *chenxt@lnut.edu.cn* (X. Chen)

powders were obtained by mechanical mixing 50Cr6Ni2Y + 1.5 wt.% TiC (named sample 1#), 50Cr6Ni2Y + 3.0 wt.% TiC (named sample 2#), and 50Cr6Ni2Y + 4.5 wt.% TiC (named sample 3#). The chemical composition of 50Cr6Ni2Y powder is shown in Table 1. High-purity TiC (99.9 %) powders were provided by Guangzhou Metal Metallurgy (Group) Co. The experimental powders were dried in a drying oven at 150 °C for 2 h before DLD. A YLS-1000-CUT-TR laser (IPG Photonics) was used to produce alloy steel samples with TiC contents from 1.5 wt.% to 4.5 wt.%, and the DLD process is shown in Fig. 1. The DLD parameters were optimized using the control variable method, with a laser power of 600 W, a scanning speed of 10 mm/s, the spot diameter of 2 mm, and an overlap rate of 30 %.

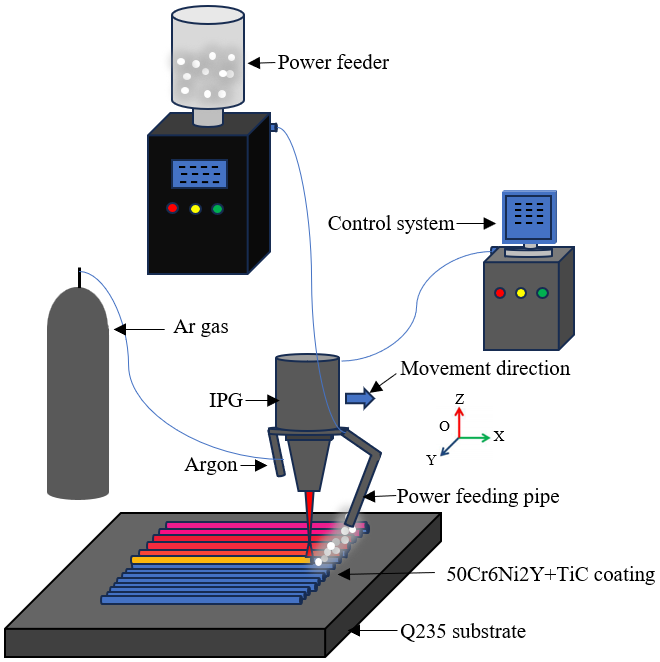

Fig. 1. Schematic diagram of the DLD coatings process

Table 1. Chemical composition of 50Cr6Ni2Y, wt.%

Element	C	Cr	Ni	Si	Mn	Y	Fe
Content	0.51	5.95	1.95	0.52	0.55	0.47	90.05

2.2. Characterization methods

Three coatings were corroded in a solution with a ratio of 2 mg $CuSO_4$ + 10 ml HCl + 10 ml H_2O. The microstructure was observed using Leica DM 2700M metallographic microscope and Sigma 500 scanning electron microscope (SEM). The coatings were analyzed at a scanning speed of 5°/min and a scanning range of 20°~90° by an Empyrean X-ray diffractometer (XRD). Microhardness of the coatings was measured using a DHV-1000AV Vickers hardness tester with a load of 1 N for 10 s. As for the wear test, a Bruker (CETR) UMT-2 reciprocating tester was used at room temperature. The friction pair was made of 4 mm diameter Al_2O_3 steel balls, with a friction speed of 70 mm/min, a friction time of 10 min, a load of 10 N, and a wear scar length of 6 mm. The wear rate of the coatings was calculated using the Eq 1:

$$\text{wear rate} = (M - m)/M \times 100\%, \quad (1)$$

where M and m are the weights of the test samples before and after wear.

3. EXPERIMENTAL RESULTS AND DISCUSSION

3.1. Microstructure of DLD 50Cr6Ni2Y coatings with different TiC contents

Fig. 2 shows metallographic photos of DLD 50Cr6Ni2Y coatings with different TiC contents. Three fabricated coatings all exhibited good bonding with the substrate. There were no obvious pores or cracks in samples 1# and 2# when TiC contents were low (1.5 wt.% and 3.0 wt.%. However, cracks as marked in Fig. 2 c can be seen in sample 3# with a TiC content of 4.5 wt.%. As a brittle strengthening phase, when TiC was added too much, the brittle stress of the coating increased, leading to the formation of cracks [15, 16].

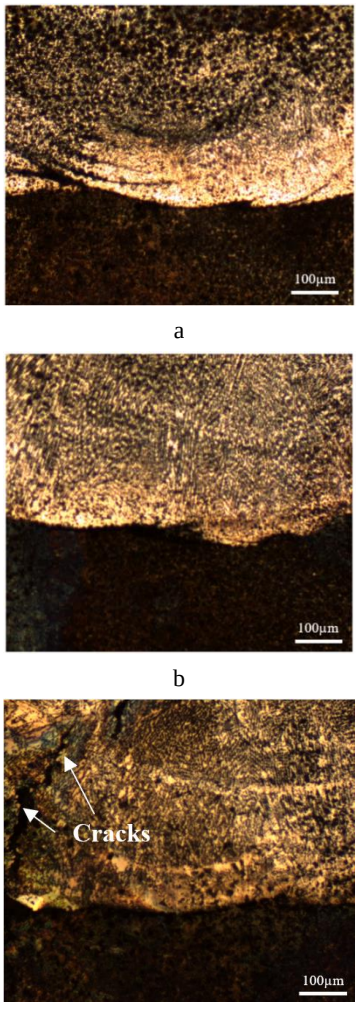

Fig. 2. Metallographic photos of DLD 50Cr6Ni2Y coatings with different TiC contents: a – 1#; b – 2#; c – 3#

Fig. 3 shows the XRD pattern of DLD 50Cr6Ni2Y coatings with different TiC contents. The phases of the coatings were α-Fe (Fe-Cr-Ti), γ-Fe (Fe-Ni), and TiC. Compared to the standard 2θ degree of α-Fe, the diffraction peaks of the α-Fe (Fe-Cr-Ti) shifted slightly to the left direction. This is due to Cr, Ni and Ti were dissolved in α-

Fe to form Fe-Cr-Ti solid solution, which caused lattice distortion. The formation of solid solution was related to the rapid cooling and solidification conditions during the DLD process. Cui [17] et al. also found that the phase stress and the laser induced thermal stress in the processing of DLD alloy steel led to lattice distortion.

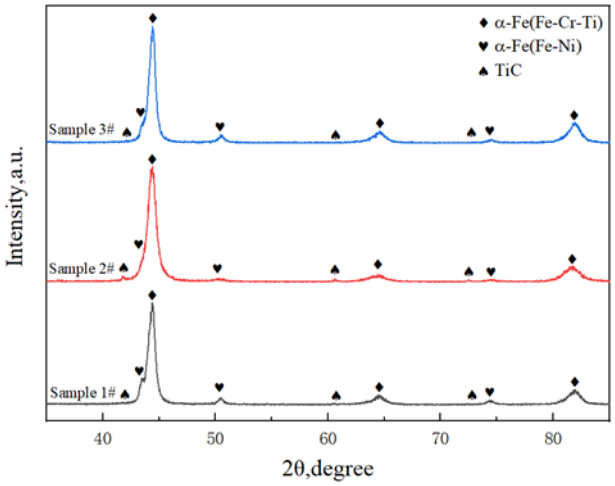

Fig. 3. XRD patterns of DLD 50Cr6Ni2Y coatings with different TiC contents

The formation of γ-Fe (Fe-Ni) was related to the repeated thermal cycling of DLD samples. Even if the temperature reaches the termination temperature of martensitic transformation, austenite cannot be completely transformed into martensite.

Fig. 4 shows SEM photos and linear scan analysis of the samples with different TiC contents. The microstructure of the fabricated coatings was mainly bainite, and irregular black particles were observed in Fig. 4 d, e. The EDS analysis results for the marked points in Fig. 4 a – e was listed in Table 2. Ti element was detected at both points A and B, indicating that some of the Ti element originating from the added TiC particles diffused into the matrix. Fig. 4 a – c shows that the addition of TiC content has no significant effect on the microstructure and size of bainite. The C and D points were rich in Ti and C elements, representing the irregular black particles in samples 2# and 3# were TiC. It is worth noting that the content of the Ti element in points D, E, and F gradually decreased. Furthermore, a similar phenomenon was also observed in the linear scan analysis results in Fig. 4 f, where the content of Ti and C elements decreased along the direction away from TiC particles. It was confirmed that TiC particles undergo melting during the deposition process. However, rapid solidification resulted in only a small amount of diffusion of Ti and C elements from the boundary of the TiC particle to the matrix.

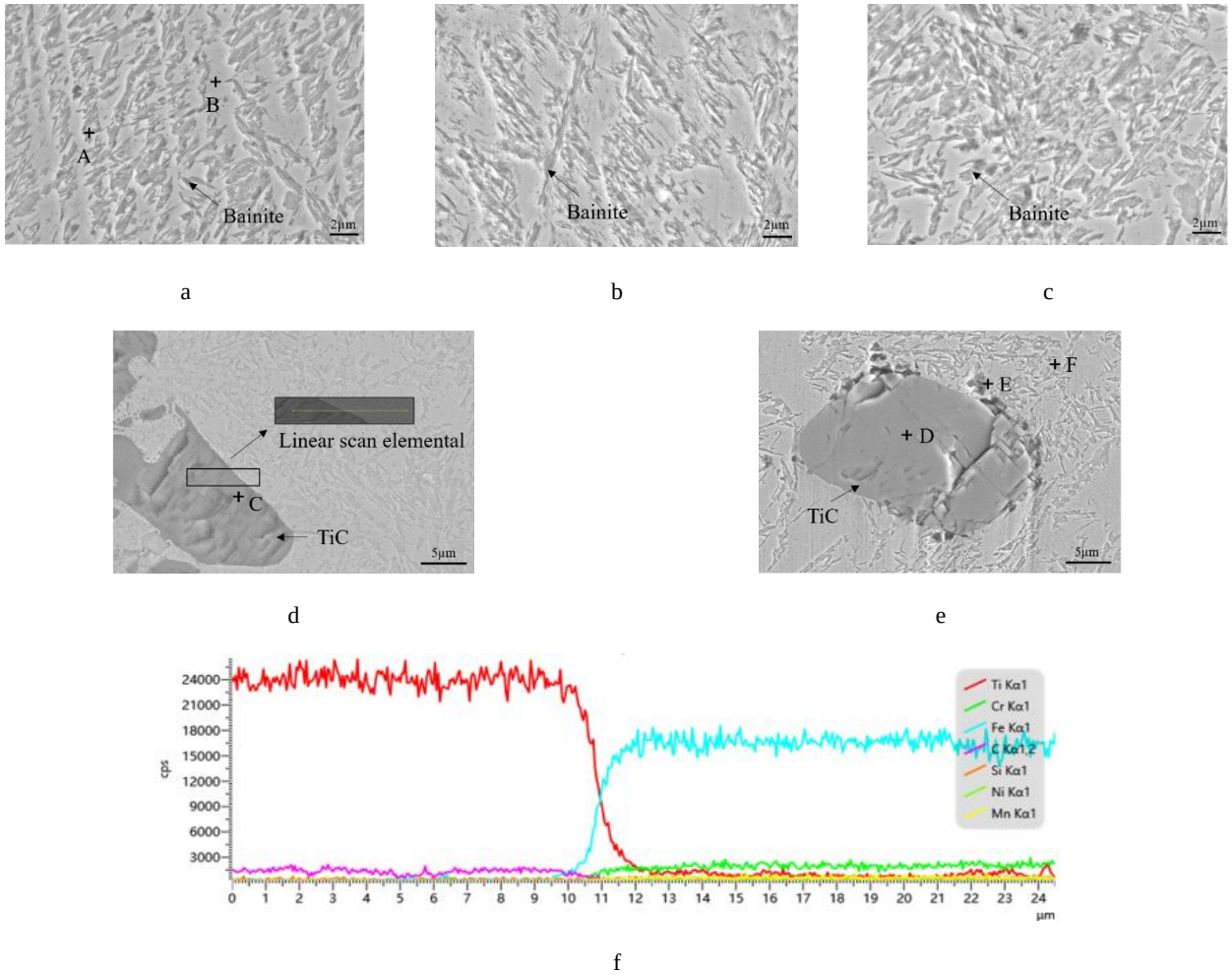

Fig. 4. SEM photos of DLD 50Cr6Ni2Y coatings with different TiC contents: a – 1#; b, d – 2#; c, e – 3#; f – linear scan elemental changes

Table 2. EDS analysis of marked points in Fig. 4, wt.%

Element	C	Fe	Ti	Remainder
A	4.88	86.47	0.54	8.11
B	7.34	85.40	0.23	7.03
C	19.64	1.38	78.98	0
D	19.07	0.65	80.28	0
E	6.71	84.23	0.93	8.13
F	5.96	85.71	0.45	7.88

Therefore, a small amount of Fe was also detected at the C and D points, and point C was closer to the boundary than point D, so the content of Fe was higher. In addition, there were obvious fractures and pores around the TiC particle in sample 3#. This is because the rheological properties of TiC particles were different from the matrix, and the excessive addition of TiC particles resulted in poor bonding with the matrix during the solidification process [18].

3.2. Properties of DLD 50Cr6Ni2Y coatings with different TiC contents

Fig. 5 displays the microhardness curves of the DLD 50Cr6Ni2Y coatings with different TiC contents. The average microhardness of the coatings was 600 ± 31.8 $HV_{0.2}$, 758 ± 23.3 $HV_{0.2}$, and 732 ± 39.7 $HV_{0.2}$, respectively, all of which were higher than that of the 50Cr6Ni2Y alloy steel without TiC (537 $HV_{0.2}$). The high hardness of the coatings was closely related to the second phase strengthening effect of TiC particles and the solid solution strengthening effect of the solid solution [19]. Therefore, for samples 1# and 2#, the more TiC added, the more significant the strengthening effect, and the higher the microhardness of the coatings. However, the excessive addition of TiC resulted in the formation of cracks in sample 3# as shown in Fig. 2 c, which reduced the microhardness of the coating.

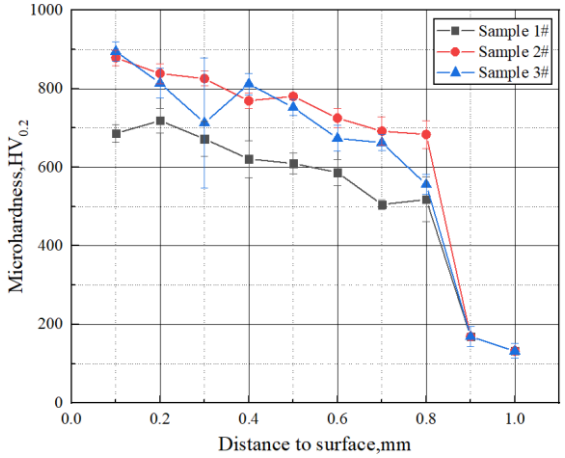

Fig. 5. Microhardness curves of the DLD 50Cr6Ni2Y coatings with different TiC contents

Fig. 6 shows the friction coefficient curves and wear scar morphology of wear scars of the coatings. The average friction coefficients of the three coatings were 0.67, 0.58, and 0.69. Generally, the lower the friction coefficient, the better the wear resistance of the coatings [20]. In Fig. 6 b – d, the cutting grooves on the worn surface of the samples indicated that the wear mechanism of these coatings is abrasive wear. The average wear rates of the coatings were calculated using Eq. 1, which were 0.88 %, 0.37 %, and 0.38 %, respectively. The added TiC can slow down the formation and expansion of wear scars, and continuously support the coating during the wear process.

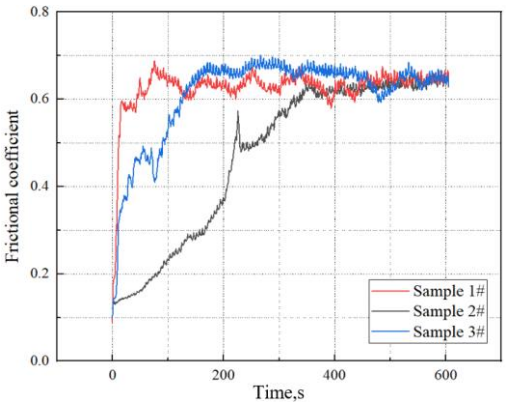

a

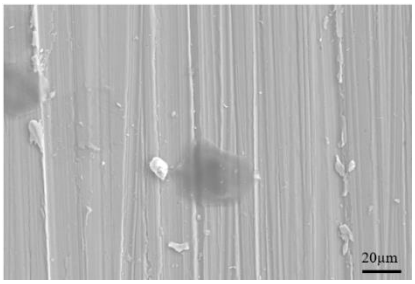

b

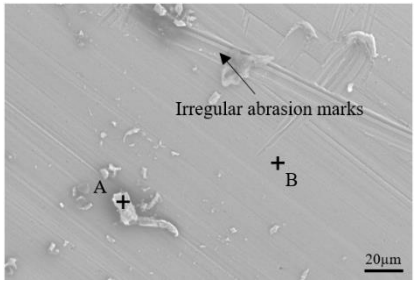

c

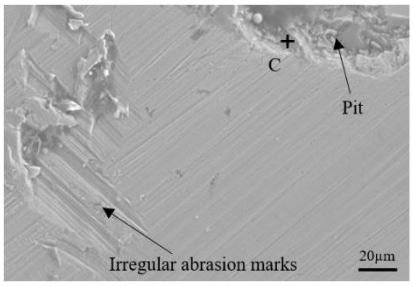

d

Fig. 6. The friction coefficient curves and wear scar morphology of DLD 50Cr6Ni2Y coatings with different TiC contents: a – friction coefficient curves; b – 1#; c – 2#; d – 3#

Therefore, the deepest grooves were observed on the surface of sample 1# with the lowest TiC content. Irregular abrasion marks can be observed in Fig. 6 c, d, and the EDS analysis results in Table 3 indicate that these marks were caused by the dragging of TiC debris during the wear process. Moreover, the poor bonding between TiC and the

matrix in sample 3# made it easier for broken TiC particles to detach from the coating, resulting in the formation of the pit in Fig. 6 d.

Table 3. EDS analysis of marked points in Fig. 6, wt.%

Element	C	Ti	Fe	O	Remainder
A	6.06	1.73	83.86	0.64	7.71
B	8.40	1.69	76.98	3.46	9.47
C	6.34	10.22	72.90	1.46	9.08

4. CONCLUSIONS

1. Three 50Cr6Ni2Y +x wt.% TiC (x = 1.5, 3.0, 4.5) coatings were successfully prepared on Q235 by DLD. The microstructure of the fabricated coatings was bainite and TiC particles, and the phases were α-Fe (Fe-Cr-Ti), γ-Fe (Fe-Ni), and TiC.
2. The embedded TiC particles not only played a second phase strengthening effect, but also formed diffusion interfaces with the matrix, allowing some Ti elements to dissolve in the matrix and play a solid solution strengthening role. The excessive addition of TiC particles resulted in poor bonding with the matrix.
3. The DLD 50Cr6Ni2Y + 3.0 wt.% TiC coating demonstrated the best properties, with a microhardness of 758 ± 23.3 $HV_{0.2}$, an average friction coefficient of 0.58, and a wear rate of 0.37 %. The high performance of the coating was closely related to the good formability, the second phase strengthening, and the solid solution strengthening effect. The results of this study could provide a reference for DLD wear-resistant coatings on alloy steel parts.

Acknowledgments

Fundamental Research Project (No. LJKMZ20220962, LJKMZ20222271 and JYTMS20230846) of the Educational Department of Liaoning Province, the Ph.D. research startup foundation of Liaoning University of Technology (No. XB2022002).

REFERENCES

1. **Zhu, L., Xue, P., Lan, Q., Meng, G., Ren, Y., Yang, Z., Xu, P., Liu, Z.** Recent Research and Development Status of Laser Cladding: A review *Optics & Laser Technology* 138 2021: pp. 106915. https://doi.org/10.1016/j.optlastec.2021.106915
2. **Li, Z., Ma, G., Zhao, H., Mou, H., Xu, J., Wang, W., Xing, Z., Li, Y., Gao, W., Wang, H.** Research Status and Prospect of Extreme High-speed Laser Cladding Technology *Optics & Laser Technology* 168 2024: pp. 109800. https://doi.org/10.1016/j.optlastec.2023.109800
3. **Tebianian, M., Aghaie, S., Razavi Jafari, N.S., Elmi Hosseini, S.R., Pereira, A.B., Fernandes, F.A., Huo, Y.** A Review of the Metal Additive Manufacturing Processes *Materials* 16 (24) 2023: pp. 7514. https://doi.org/10.3390/ma16247514
4. **Xie, L., Wang, Y.** Microstructure and Mechanical Properties of Fe-Based Alloy Coatings Fabricated by Laser Cladding *Materials Science* 29 (4) 2023: pp. 456 – 462. https://doi.org/10.5755/j02.ms.33919
5. **Gusarov, A.V., Yadroitsev, I**. Laser Additive Manufacturing of Metal Parts: Modeling, Materials, Printing, and Applications *Advanced Materials Research* 1148 2018: pp. 95 – 118. https://doi.org/10.4028/www.scientific.net/amr.1148.95
6. **Chen, X., Chen, S., Cui, T., Liang, J., Liu, C., Wang, M.** A New 50Cr6Ni2Y Alloy Steel Prepared by Direct Laser Deposition: Its Design, Microstructure, and Properties *Optics and Laser Technology* 126 2020: pp. 106080. https://doi.org/10.1016/j.optlastec.2020.106080
7. **Gu, Y., Xia, K., Wu, D., Mou, J., Zheng, S.** Technical Characteristics and Wear-resistant Mechanism of Nano Coatings: a review *Coatings* 10 (3) 2020: pp. 233. https://doi.org/10.3390/coatings10030233
8. **Zeng, J., Lian, G., Chen, C., Huang, X.** Influences of the TiC composite introduction method on the microstructures and properties of Nickel-Based coatings *Optics & Laser Technology* 156 2022: pp. 108633. https://doi.org/10.1016/j.optlastec.2022.108633
9. **Chen, L., Zhao, Y., Meng, F., Yu, T., Ma, Z., Qu, S., Sun, Z.** Effect of TiC Content on the Microstructure and Wear Performance of in Situ Synthesized Ni-based Composite Coatings by Laser Direct Energy Deposition *Surface and Coatings Technology* 444 2022: pp. 128678. https://doi.org/10.1016/j.surfcoat.2022.128678
10. **Ao, S., Wang, T., Huang, Y., Dai, Y., Luo, Z.** The Wear Properties of TiC/Al-based Composite Coating Applied by Laser Cladding *Metals* 8 (11) 2018: pp. 975. https://doi.org/10.3390/met8110975
11. **Cai, Y., Luo, Z., Feng, M., Liu, Z., Huang, Z., Zeng, Y.** The Effect of TiC/AlO Composite Ceramic Reinforcement on Tribological Behavior of Laser Cladding Ni60 Alloys Coatings[23] *Surface and Coatings Technology* 291 2016: pp. 222 – 229. https://doi.org/10.1002/adem.201800966
12. **Xu, X., Mi, G., Xiong, L.** Morphologies, Microstructures and Properties of TiC Particle Reinforced Inconel 625 Coatings Obtained by Laser Cladding with Wire *Journal of Alloys and Compounds* 740 2018: pp. 16 – 27. https://doi.org/10.1016/j.jallcom.2018.02.149
13. **Zhang, H., Wang, L., Zhang, S.** An Investigation on Wear and Cavitation Erosion-Corrosion Characteristics of the TiC Modified Fe-Based Composite Coating via Laser Cladding *Journal of Materials Research and Technology* 23 2023: pp. 6162 – 6173. https://doi.org/10.1016/j.jmrt.2023.09.177
14. **Liu, Y., Xie, D., Lv, F.** Strength Enhancement of Laser Powder Bed Fusion 316L by Addition of Nano TiC Particles *Materials* 17 (5) 2024: pp. 1129. https://doi.org/10.3390/ma17051129
15. **He, X., Song, R., Kong, D.** Effects of TiC on the Microstructure and Properties of TiC/TiAl Composite Coating Prepared by Laser Cladding *Optics & Laser Technology* 112 2019: pp. 339 – 348. https://doi.org/10.1016/j.optlastec.2018.11.037
16. **Wu, G., Wang, D., Liu, X., Wang, M., Chen, D., Wu, Y., Shen, D.** New Formation Mechanisms of Pores and Cracks in Micro-arc Oxidation Coatings on 6061 Aluminum Alloy with High Temperature Oxide Prefab Film *Materials Science (Medžiagotyra)* 27 (1) 2021: pp. 37 – 41. https://doi.org/10.5755/j02.ms.24210
17. **Cui, X., Zhang, S., Wang, C., Zhang, C.H., Chen, J., Zhang, J.B.** Microstructure and Fatigue Behavior of a Laser Additive Manufactured 12CrNi2 Low Alloy Steel *Materials Science and Engineering* 766 2019: pp. 138685. https://doi.org/10.1016/j.msea.2019.138685
18. **Eastgate, R.M., Moore, J.E.** Deformation Behavior of

Nanoporous Polycrystalline Silver. Part I: Microstructure and Mechanical Properties *Acta Materialia* 131 2017: pp. 467 – 474. https://doi.org/10.1016/j.actamat.2017.04.021

19. **Wang, Z., Cheng, H., Lv, Y., Zhang, Z., Fan, J., Zhang, H., Liu, B., Ma, Z.** Effect of TiC content on the Microstructure and Mechanical Properties of Ti-30Mo-xTiC Composites *International Journal of Refractory Metals and Hard Materials* 107 2022: pp. 105879. https://doi.org/10.1016/j.ijrmhm.2022.105879
20. **Zheng, D., Zhao, X., An, K., Chen, L., Zhao, Y., Khan, D.F., Qu, X., Yin, H.** Effects of Fe and Graphite on Friction and Wear Properties of Brake Friction Materials for High-speed and Heavy-Duty Vehicles *Tribology International* 2022: pp. 108061. https://doi.org/10.1016/j.triboint.2022.108061